Research Square

Preprints are preliminary reports that have not undergone peer review.
They should not be considered conclusive, used to inform clinical practice,
or referenced by the media as validated information.

Interpretable Reference Evapotranspiration Estimation Model Combining Multi-Strategy Crested Porcupine Optimizer and CNN-LSTM

Xu Yao
Jilin Agricultural University
Yingnan Wang
Wangyingnan2026@outlook.com

Jilin Agricultural University
Jingji Liu
Jilin Agricultural University
Jiaxuan Shi
Jilin Agricultural University
Kelun Ma
Jilin Agricultural University
Xuerui Li
Jilin Agricultural University

Article

Keywords: CNN-LSTM, reference evapotranspiration estimation, hyperparameter optimization, SHAP interpretability, time series modeling

Posted Date: May 13th, 2026

DOI: https://doi.org/10.21203/rs.3.rs-9547130/v1

License: This work is licensed under a Creative Commons Attribution 4.0 International License.
Read Full License

Additional Declarations: No competing interests reported.

Interpretable Reference Evapotranspiration Estimation Model Combining Multi-Strategy Crested Porcupine Optimizer and CNN-LSTM

Xu Yao[1a], Yingnan Wang[1]*, Jingji Liu[1b], Jiaxuan Shi[1c], Kelun Ma[1d], Xuerui Li[1e]

1. College of Engineering and Technology, Jilin Agricultural University, Changchun, 130118, China;

aEmail: Yaoxu20262026@outlook.com

bEmail: Liujingji@outlook.com

cEmail: Shijiaxuan2026@outlook.com

dEmail: Makelun2026@outlook.com

eEmail: Lixuerui2026@outlook.com

*Email: Wangyingnan2026@outlook.com

Abstract： High-precision estimation of reference evapotranspiration (ET_0) is an important foundation for agricultural irrigation regulation and regional water resource optimization management. This paper proposes a hybrid model that integrates Convolutional Neural Network (CNN) and Long Short-Term Memory (LSTM), combined with the Adaptive Cauchy-Simulated Annealing hybrid Crested Porcupine Optimizer (ACSA-CPO) to globally optimize key hyperparameters of the model for ET_0 estimation. ET_0 is calculated by the Penman–Monteith (PM) formula and used as the reference baseline for model training and evaluation. The model extracts local temporal features of meteorological time series through CNN and captures long-term temporal dependencies using LSTM, thereby improving the model's ability to model complex nonlinear processes. The ACSA-CPO enhances the hyperparameter search capability effectively by introducing a multi-strategy collaborative optimization mechanism, further improving the model's estimation accuracy for ET_0. Experiments are conducted based on daily meteorological data of Changchun, Jilin Province from 2020 to 2025 in the ERA5 reanalysis dataset. The results show that the proposed model achieves superior performance in the rapid ET_0 estimation task, with Mean Absolute Error (MAE), Root Mean Square Error (RMSE), Mean Absolute Percentage Error (MAPE), coefficient of determination (R^2) and Nash-Sutcliffe Efficiency (NSE) of 1.753 mm/day, 2.174 mm/day, 18.3%, 0.8713 and 0.859, respectively.

Comparative experiments with Particle Swarm Optimization (PSO) and Sparrow Search Algorithm (SSA) and ablation analysis further verify the effectiveness and stability of the proposed model. In addition, the Shapley Additive Explanations (SHAP) method is used for model interpretability analysis. The results indicate that the impacts of meteorological variables on ET_0 present obvious nonlinear characteristics, among which solar radiation, wind speed and air temperature make differentiated contributions to ET_0 in different value ranges, thus providing a more physically meaningful interpretation for the model estimation results. This study provides an effective data-driven scheme for rapid reference evapotranspiration estimation and agricultural water resource management, especially offering technical support for efficient ET_0 acquisition under the condition of missing meteorological data.

Keywords: CNN-LSTM; reference evapotranspiration estimation; hyperparameter optimization; SHAP interpretability; time series modeling

1. Introduction

Northeast China, as an important grain production base in China, is dominated by corn planting in its agricultural production mode, with an output accounting for about 30% of the national total output, playing a key role in ensuring national food security [1][2]. However, restricted by uneven regional water resource distribution and low utilization efficiency, the sustainable development of this production mode faces severe challenges [3]. Reference evapotranspiration (ET_0), as the core link of farmland water cycle, is an important indicator for measuring crop water demand and formulating irrigation strategies, accounting for more than 90% of crop water consumption [4]. Therefore, achieving high-precision estimation of ET_0 is of great significance for improving agricultural water use efficiency and optimizing irrigation management [5][12].

Among traditional methods, the Penman–Monteith (PM) model is recommended by the Food and Agriculture Organization (FAO) as the standard method for calculating reference evapotranspiration. By comprehensively considering meteorological factors such as temperature, humidity, wind speed and radiation, it has high applicability and reliability in Northeast China [13]. However, such physical models rely heavily on the integrity and quality of input meteorological data, limiting their application under complex meteorological conditions or data missing scenarios, and are difficult to effectively characterize the complex nonlinear coupling relationship among

multiple meteorological factors. With the development of artificial intelligence technology, deep learning models have shown significant advantages in the field of rapid ET_0 estimation. Among them, Long Short-Term Memory (LSTM) has been widely used in reference evapotranspiration estimation research due to its unique gating mechanism that can effectively capture long-term dependencies in time series [14][16]. Nevertheless, the single LSTM model still has limitations in extracting local dynamic features and processing multi-scale changes. To this end, researchers have introduced Convolutional Neural Network (CNN) to construct a CNN-LSTM hybrid model to enhance the model's joint modeling ability of local features and long-term dependencies, thereby improving ET_0 estimation accuracy [17][18].

Although the CNN-LSTM model shows strong capability in ET_0 prediction, its performance is highly dependent on hyperparameter settings. Traditional optimization methods (such as grid search and random search) are prone to local optima and have limited search efficiency, restricting further improvement of model performance. In recent years, the Crested Porcupine Optimizer (CPO), as an emerging meta-heuristic algorithm, has demonstrated strong global search ability in high-dimensional nonlinear optimization problems [19]. However, the original CPO still has deficiencies in population initialization and perturbation mechanism, which easily lead to premature convergence in the search process and affect the optimization effect [20].

To address the above problems, this paper constructs a rapid ET_0 estimation model integrating the ACSA-CPO optimization strategy and CNN-LSTM. ET_0 is calculated by the Penman–Monteith (PM) formula and used as the reference baseline for model training and evaluation. By introducing a multi-strategy collaborative optimization mechanism, the proposed method effectively improves the model's hyperparameter search capability and ET_0 estimation accuracy. Meanwhile, the SHAP method is combined to conduct interpretability analysis on the model to reveal the influence mechanism of meteorological variables on ET_0 estimation results. The main contributions of this paper are as follows:

(1) This paper constructs a hybrid model integrating multi-scale one-dimensional Convolutional Neural Network (1D-CNN) and LSTM to realize collaborative modeling of local features and long-term dependencies of meteorological time series, thereby improving ET_0 estimation accuracy;

(2) This paper proposes the ACSA-CPO hyperparameter optimization strategy, which

enhances global search capability and suppresses premature convergence through the synergy of Latin hypercube initialization, adaptive perturbation mechanism and simulated annealing acceptance criterion, thus improving the model's generalization performance in complex nonlinear problems;

(3) This paper introduces a SHAP-based interpretability analysis framework to quantitatively reveal the nonlinear contribution characteristics of meteorological variables to ET_0 at the model level and verify its consistency with the physical mechanism of the PM equation.

2. Materials and Methods

2.1 Methodology

The Penman-Monteith method is the standard method recommended by the Food and Agriculture Organization (FAO) for calculating reference crop evapotranspiration [21]. Based on the energy balance principle and water vapor diffusion theory, this method comprehensively considers the impacts of meteorological factors such as radiation, air temperature, humidity and wind speed on the evapotranspiration process. Its basic formula is as follows:

$$ET_O = \frac{0.408\Delta(R_n - \mathrm{G}) + \gamma \frac{900}{T + 273} u_2 (e_s - e_a)}{\Delta + \gamma(1 + 0.34u_2)} \quad (1)$$

Where: ET_O is reference crop evapotranspiration (mm/d);R_n is net solar radiation (MJ/m² /d); G is soil heat flux (MJ/m² /d);T is average air temperature (° C);u_2 is average wind speed at 2 m height (m/s);e_s is saturated vapor pressure (kPa);e_a is actual vapor pressure (kPa);Δ is the slope of the relationship curve between saturated vapor pressure and temperature (kPa/° C);γ is the psychrometric constant (kPa/° C).

2.2 Convolutional Neural Network

Convolutional Neural Network (CNN) is a deep learning architecture that can automatically extract spatial features through local receptive fields, especially good at processing data with grid topology [22]. As shown in Figure 2.1, a typical CNN consists of an input layer, convolutional layer, activation function, pooling layer and fully connected layer. Its core logic is to capture local features through the sliding operation of convolution kernels, then introduce nonlinear activation functions (such as ReLU) to break linear constraints and enhance the model's feature expression ability; the pooling layer reduces dimensions while retaining key features through downsampling, and finally maps to the output space through the fully connected layer [23].

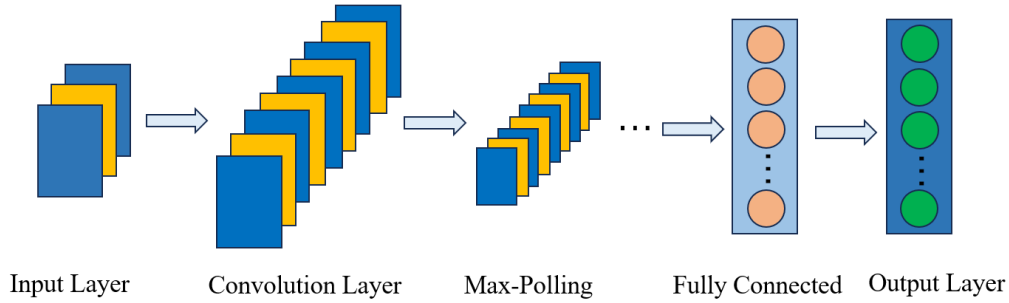


Figure 2.1 CNN Architecture

The calculation formulas of convolution operation and pooling process are as follows:

$$C_i = f(C_{i-1} * W_i + b_i) \tag{2}$$

$$d_i = \max(c_1, c_2, \ldots, c_n) \tag{3}$$

Where C_i and C_{i-1} represent the feature outputs of the i-th and $i-1$-th layers respectively, W_i represents the weight vector, b_i represents the bias of the i-th layer, d_i is the feature extracted by the convolutional layer, and n is the pooling width.

2.3 Long Short-Term Memory Network

Long Short-Term Memory (LSTM) effectively alleviates the gradient vanishing and exploding problems faced by traditional Recurrent Neural Networks (RNN) when processing long sequence data by introducing a "Memory Cell" and gating mechanism [24]. As shown in Figure 2.2, its core lies in the collaborative work of forget gate, input gate and output gate. The gating units realize selective control of information flow through the Sigmoid activation function, eliminating redundant interference and retaining key long-range features. This unique architecture enables LSTM to capture complex temporal dependencies while maintaining long-term stability of internal states, thus exhibiting excellent performance in sequence modeling and trend prediction [25].

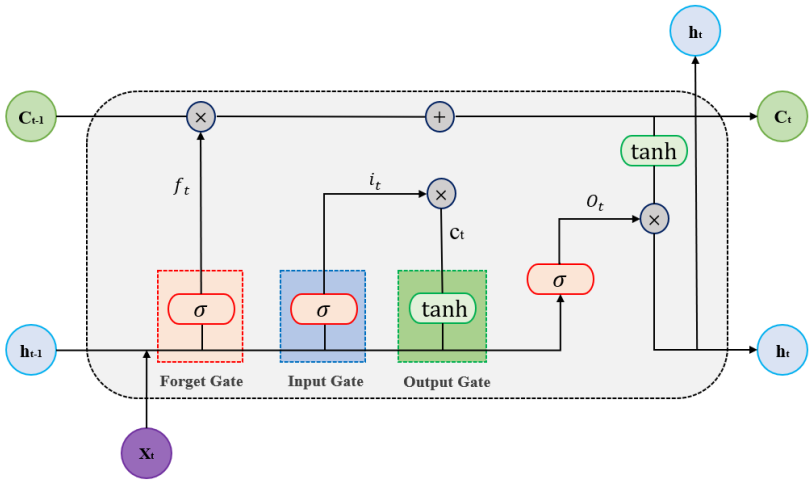


Figure 2.2 LSTM Architecture

The calculation formulas of input gate, forget gate and output gate are as follows:

$$f_t = \sigma\left(W_f \cdot [H_{t-1}, X_t] + b_f\right) \tag{4}$$

$$i_t = \sigma(W_i \cdot [H_{t-1}, X_t]) + b_i \tag{5}$$

$$g = \tanh\left(W_g \cdot [H_{t-1}, X_t] + b_g\right) \tag{6}$$

$$C_t = f \times C_{t-1} + i \times g \tag{7}$$

$$O_t = \sigma(W_o \cdot [H_{t-1}, X_t] + b_o) \tag{8}$$

$$H_t = O_t \times \tanh(G_t) \tag{9}$$

Where f_t, i_t and O_t represent the outputs of forget gate, input gate and output gate respectively; X_t represents the current input feature; C_t represents the current memory cell state; C_{t-1} is the memory cell state at the previous moment; H_t is the output state; H_{t-1} is the output state at the previous moment. W_f ,W_i ,W_o and W_g represent the input weight matrices of forget gate, input gate, output gate and candidate cell respectively. b_f ,b_i,b_o and b_g represent the bias terms of forget gate, input gate, output gate and memory gate respectively. σ represents the Sigmoid activation function, and $\tanh$ is the hyperbolic tangent activation function.

2.4 CNN-LSTM Hybrid Model

In this study, a hybrid deep learning model based on CNN-LSTM is constructed to mine the complex nonlinear relationship between meteorological variables and crop evapotranspiration, as shown in Figure 2.3. As a typical multivariate time series, meteorological data not only have coupling relationships among multiple factors, but also have significant temporal dependence. Therefore, this paper combines the advantages of Convolutional Neural Network (CNN) and Long Short-Term Memory (LSTM) to realize collaborative modeling of local dynamic features and

long-term temporal dependencies.

Specifically, the model first constructs the multivariate meteorological time series into a three-dimensional input structure, i.e., "number of samples × time steps × number of features". In the CNN module, one-dimensional convolution (1D-CNN) is used to perform sliding window convolution operations on time series data to extract local variation characteristics of meteorological variables on a short time scale. The convolutional layer adopts a parallel structure of multi-scale convolution kernels (3×1 and 5×1) to capture variation patterns at different time scales, thereby enhancing the model's ability to express short-term fluctuation features. Then, the maximum pooling layer downsamples the feature map to reduce feature dimension while suppressing noise interference and reducing model computational complexity. In this process, the temporal dimension structure is effectively preserved, so that the extracted feature sequence can be further used for subsequent temporal modeling.

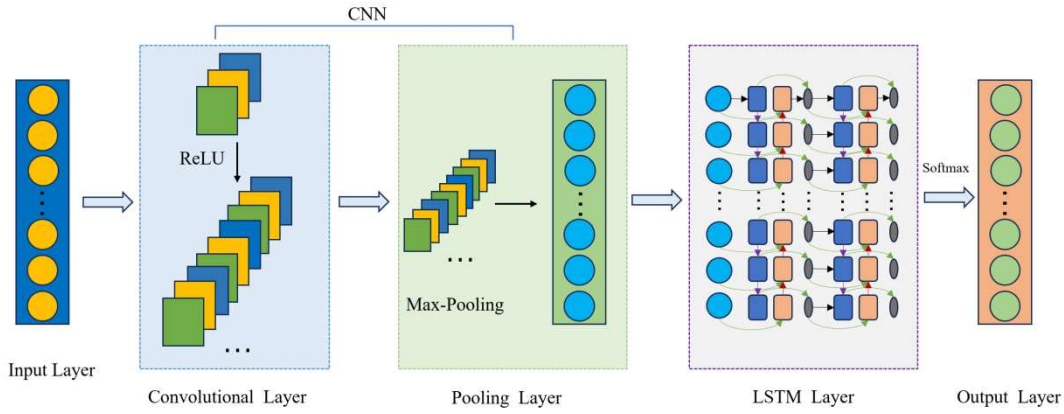


Figure 2.3 Structure of the CNN-LSTM Hybrid Model

The output features of the CNN convolutional layer X_i are expressed as follows:

$$X_i = \sigma\left(\sum_{t=0}^{k-1}(W_t \cdot X_{i+t} + b)\right) \tag{10}$$

Where X_i is the feature value of the i-th time step of the output sequence, $\sigma(\cdot)$ is the activation function, k is the convolution kernel size, W_t is the weight of the convolution kernel, X_{i+t} is the feature within the sliding window of the input sequence, and b is the bias term.

After the CNN module extracts local temporal features, the output feature sequence is input to the LSTM layer. LSTM dynamically regulates information flow through input gate, forget gate and output gate, thus effectively capturing long-term temporal dependencies in the process of

evapotranspiration change. This structure can alleviate the gradient vanishing problem of traditional recurrent neural networks in long sequence training and improve the model's ability to express temporal dynamic changes. Finally, the high-dimensional features output by LSTM are mapped through the fully connected layer to obtain the final evapotranspiration estimation value.

Although the CNN-LSTM model has strong capability in temporal feature modeling, its performance is sensitive to hyperparameter settings and is prone to local optima during training. Meanwhile, when processing long time series data, the model still has a certain risk of overfitting, which affects its generalization performance [26][27]. To further improve the model's optimization ability, this paper introduces CPO to optimize key hyperparameters of the model in the follow-up, so as to enhance the model's global search ability and improve estimation accuracy.

2.5 Crested Porcupine Optimizer

2.5.1 Introduction to the Crested Porcupine Optimizer

The Crested Porcupine Optimizer (CPO) simulates the defense mechanism of crested porcupines, and its working process is divided into two stages: global exploration and local development, corresponding to four defense strategies respectively, including visual defense, auditory defense, olfactory defense and physical attack [28]. When a crested porcupine finds a predator, it erects its quills to deter and observe whether the predator continues to approach, which is its first defense mechanism. This behavior can be expressed by Formula (11). If the predator approaches further, the crested porcupine will strengthen the exploration of the area between the two, thus accelerating convergence. On the other hand, if the predator retreats, the crested porcupine will explore a larger area to find a better solution.

$$\overrightarrow{x_i^{t+1}} = \overrightarrow{x_i^t} + \tau_1 \times \left|2 \times \tau_2 \times \overrightarrow{x_{CP}^t} - \overrightarrow{y_i^t}\right| \tag{11}$$

Where $\overrightarrow{x_i^t}$ represents the position of the i-th predator in the t-th iteration, $\overrightarrow{x_{CP}^t}$ represents the optimal solution within the current search range, $\overrightarrow{y_i^t}$ represents the position of the predator in the t-th iteration, and τ_1 and τ_2 are random values between 0 and 1 following a normal distribution.

If the predator continues to approach, the crested porcupine will make a sound to deter. Formula (12) is used to simulate the predator's reaction after hearing the sound, considering three situations: whether to continue approaching, stay still or retreat.

$$\overrightarrow{x_i^{t+1}} = \left(1 - \overrightarrow{U_1}\right) \times \overrightarrow{x_i^t} + \overrightarrow{U_1} \times \left(\vec{y} + \tau_3 \times \left(\overrightarrow{x_{r1}^t} - \overrightarrow{x_{r2}^t}\right)\right) \quad (12)$$

Where $\overrightarrow{U_1}$ is a randomly generated binary vector that can represent the potential probabilities of the three situations, $r1$ and $r2$ represent two random integers between 1 and N, and τ_3 is a random value between 0 and 1.

The first two defense strategies are the global exploration stage of CPO, while the development stage is further realized through olfactory defense and physical attack. Olfactory defense means that the crested porcupine secretes a foul smell to prevent the predator from approaching further, expressed by Formula (13). This mechanism considers the exploration of the current solution in the local area and reduces the risk of falling into local optimal solutions.

$$\overrightarrow{x_i^{t+1}} = \left(1 - \overrightarrow{U_1}\right) \times \overrightarrow{x_i^t} + \overrightarrow{U_1} \times \left(\overrightarrow{x_{r1}^t} + S_i^t \times \left(\overrightarrow{x_{r2}^t} - \overrightarrow{x_{r3}^t}\right) - \tau_3 \times \vec{\delta} \times \gamma_t \times S_i^t\right) \quad (13)$$

Where $r3$ is defined in the same way as $r1$ and $r2$, $\vec{\delta}$ is a parameter controlling the search direction, S_i^t represents the odor diffusion coefficient, and $\overrightarrow{F_i^t}$ represents the porcupine's defense strategy when simulating the physical attack of the i-th predator.

Physical attack means that the crested porcupine attacks the predator with its quills, which can strengthen the search for the current optimal solution and quickly converge to the optimal solution. This process can be expressed by Formula (14):

$$\overrightarrow{x_i^{t+1}} = \overrightarrow{x_{CP}^t} + (\alpha(1 - \tau_4) + \tau_4) \times \left(\delta \times \overrightarrow{x_{CP}^t} - \overrightarrow{x_i^t}\right) - \tau_5 \times \delta \times C \times \overrightarrow{F_i^t} \quad (14)$$

Where α is the convergence rate factor, and τ_4 and τ_5 are random values between 0 and 1.

2.5.2 Improvement of the Crested Porcupine Optimizer

Population initialization in the Crested Porcupine Optimizer (CPO) is usually generated randomly, which may lead to uneven initial distribution of the population, thus affecting the global search ability and convergence speed of the algorithm. In addition, in the defense mechanism of traditional CPO, the update of perturbation strategy is relatively fixed and lacks adaptability, resulting in unstable algorithm performance when dealing with different types of optimization problems and hindering the achievement of optimal search performance. When applying traditional CPO to high-dimensional complex search spaces in this paper, it is difficult to efficiently search the entire space, easily fall into local optima, and fail to find the global optimal

solution. Therefore, this paper makes the following improvements to traditional CPO:

(1) To ensure that the initial population uniformly covers the entire high-dimensional search space and reduce search bias caused by random initialization. This paper introduces Latin Hypercube Sampling (LHS) to initialize the CPO population, ensuring that sampling points in each dimension are uniformly distributed within their respective intervals, making individuals more balanced in the search space. The original random sampling method is expressed as Formula (15):

$$X_i = rand(X_{min}, X_{max}) \tag{15}$$

The LHS initialization method is expressed as Formula (16):

$$X_i = X_{min} + (X_{max} - X_{min}) \times \frac{\pi_i}{N} \tag{16}$$

Where X_{min} and X_{max} are variable ranges, π_i is the quantile generated by LHS, and N is the population size. LHS ensures that the population uniformly covers the entire search space, improves global search ability, avoids the initial population concentrating in certain areas, and reduces the possibility of local optima.

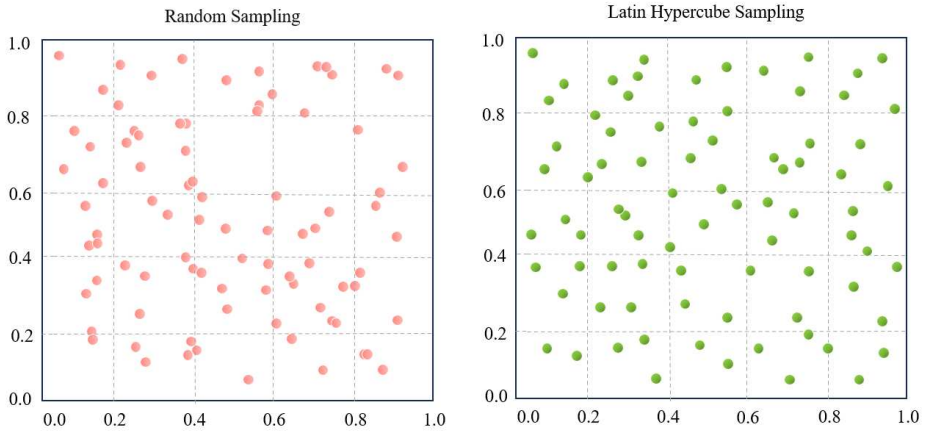


Figure 2.4 Random Sampling and Latin Hypercube Sampling

(2) This paper applies Adaptive Cauchy-Gaussian Hybrid Perturbation (ACGH) to CPO. By dynamically fusing the perturbation strategies of Cauchy distribution (global exploration) and Gaussian distribution (local development) to replace the original normal distribution perturbation, it enhances the algorithm's search space ability and ability to maintain population diversity. This process can be expressed by Formulas (17)-(21). This method uses the heavy-tailed characteristic of Cauchy distribution to jump out of local optima and avoid premature convergence; in the later

stage of iteration, it refines convergence through Gaussian distribution, balances search efficiency and improves robustness; and adaptively adjusts perturbation parameters according to the algorithm process, reducing the need for manual parameter tuning.

$$\overrightarrow{x_i^{t+1}} = \left(1 - \overrightarrow{U_1}\right) \times \overrightarrow{x_i^t} + \overrightarrow{U_1} \times \left(\overrightarrow{x_{r1}^t} + S_i^t \times \left(\overrightarrow{x_{r2}^t} - \overrightarrow{x_{r3}^t}\right) - \Delta x \times \vec{\delta} \times S_i^t\right) \tag{17}$$

$$\Delta x = \begin{cases} \gamma \cdot \sigma(t) \cdot C(0,1) & w_{Cauchy}(t) \\ \sigma(t) \cdot N(0,1) & w_{Gaussian}(t) \end{cases} \tag{18}$$

$$\sigma(t) = \sigma_{init} \cdot e^{-\lambda t} \tag{19}$$

$$w_{Cauchy}(t) = 1 - \frac{t}{T} \tag{20}$$

$$w_{Gaussian}(t) = \frac{t}{T} \tag{21}$$

Where Δx and δ are perturbation terms, $\sigma(t)$ is the dynamic step size, which decays exponentially with the number of iterations t, balancing early exploration and later development, and γ is the Cauchy perturbation scaling factor (default 3~5). $w_{Cauchy}(t)$ is the Cauchy weight, $w_{Gaussian}(t)$ is the Gaussian weight, T is the maximum number of iterations. In the early stage of iteration $(t \ll T)$, Cauchy perturbation is dominant, and in the later stage $(t \to T)$, it transitions to Gaussian perturbation.

(3) This paper introduces a hybrid strategy of Simulated Annealing (SA) acceptance criterion. By accepting inferior solutions, it avoids premature convergence of the algorithm to local optima and enhances global search ability. The SA acceptance criterion mainly acts on the acceptance stage of the solution after the new solution is generated by the defense mechanism. It maintains population diversity by probabilistically accepting inferior solutions and avoids premature convergence. Its core is that the temperature parameter T decays with the number of iterations t. The high-temperature stage (early iteration) accepts more inferior solutions for extensive exploration, and the low-temperature stage (later iteration) gradually focuses on the development of high-quality solutions, dynamically balancing exploration and development, and further improving the robustness of the algorithm. This process is expressed by Formulas (22)-(24).

SA acceptance probability formula (Metropolis criterion):

$$P(accept) = \begin{cases} 1 & ,if \quad f(X_{new}) \le f(X_{old}) \\ \exp\left(-\dfrac{f(X_{new}) - f(X_{old})}{T(t)}\right) & ,otherwise. \end{cases} \tag{22}$$

Temperature decay formula:

$$T(t) = T_0 \cdot \gamma^t \tag{23}$$

Improved defense mechanism update rule formula:

$$\overrightarrow{x_i^{t+1}} = \begin{cases} \overrightarrow{x_i^{t+1}}_{candidate} & \text{以概率} P(accept) \\ \overrightarrow{x_i^{t+1}} & \text{以概率 } 1 - P(accept) \end{cases} \tag{24}$$

Where $f(X_{new})$ and $f(X_{old})$ are the fitness values of the new solution and the old solution, T_0 is the initial temperature, t is the current number of iterations, and γ is the temperature decay rate ($\gamma \in (0,1)$, usually 0.95~0.99).

Due to various improvements to the traditional CPO algorithm in population initialization strategy, perturbation mechanism and acceptance criterion, the improved algorithm is named Adaptive Cauchy-Simulated Annealing hybrid Crested Porcupine Optimizer (ACSA-CPO). Compared with traditional CPO, ACSA-CPO improves the uniformity of population initialization by introducing Latin hypercube sampling, enhances global exploration and local development capabilities through adaptive Cauchy-Gaussian hybrid perturbation, and improves the ability to jump out of local optima combined with simulated annealing acceptance criterion. The above improvements act through a collaborative mechanism, effectively improving the search efficiency, convergence performance and robustness of the algorithm in high-dimensional complex optimization problems.

2.6 Multi-Strategy Hyperparameter Optimization Method

To further improve the performance of the CNN-LSTM model in crop evapotranspiration prediction, this paper introduces ACSA-CPO to optimize key hyperparameters of the CNN-LSTM model. In this study, the structural parameters of the CNN-LSTM model remain fixed during training to define the basic architecture of the model, thus focusing the optimization process on the impact of training hyperparameters on model performance. The specific settings are shown in Table 2.1, including the number of CNN convolutional layers, the number of convolution kernels, multi-scale convolution kernel sizes, and the number of LSTM layers.

Table 2.1 Structural parameters of the CNN-LSTM model

Model Structure	Parameter Settings
CNN	Conv, Max pooling
CNN convolution layers	3

CNN filters per layer	128
CNN convolution core size	3×1, 5×1
LSTM layers	2
LSTM layer units	64
Activation function	Relu

The above search ranges are set based on experience and reasonably constrained in combination with model stability and computational efficiency. On this basis, the ACSA-CPO algorithm is used to optimize key hyperparameters during model training to improve model prediction accuracy and generalization ability. The hyperparameters to be optimized include Learning Rate, Dropout Rate, Batch Size and L2 regularization coefficient, and the optimal results are shown in Table 2.2.

In the optimization process, each individual represents a set of candidate hyperparameter combinations, which can be expressed as:

$$X_i = [lr, Dropout, Batch\ Size, L2\ ] \tag{25}$$

Where lr represents learning rate, $Dropout$ represents $Dropout$ rate, $Batch\ Size$ represents batch size, and $L2$ represents $L2$ regularization coefficient. To evaluate the pros and cons of different hyperparameter combinations, a fitness function needs to be constructed. This paper uses the prediction error of the model on the validation set as the fitness evaluation index, adopts Mean Absolute Error (MAE) as the objective function. Since the optimization goal is to improve prediction accuracy, the optimization problem can be expressed as:

$$minf(X_i) = MAE \tag{26}$$

That is, the ACSA-CPO algorithm is used to find the optimal hyperparameter combination that minimizes the validation set MAE within a given parameter search space. The overall framework of the ACSA-CPO algorithm optimizing key hyperparameters of the CNN-LSTM model is shown in Figure 2.5.

Table 2.2 Optimal hyperparameters obtained by ACSA-CPO optimization and their search ranges

Hyperparameters	Optimal value	Search scope
Learning Rate	0.0012	0.0001 - 0.01
Dropout Rate	0.25	0.1 - 0.5
Batch Size	64	16 - 128
L2 Regularization	0.0004	1e-5 - 1e-3

Fitness function	MAE	-

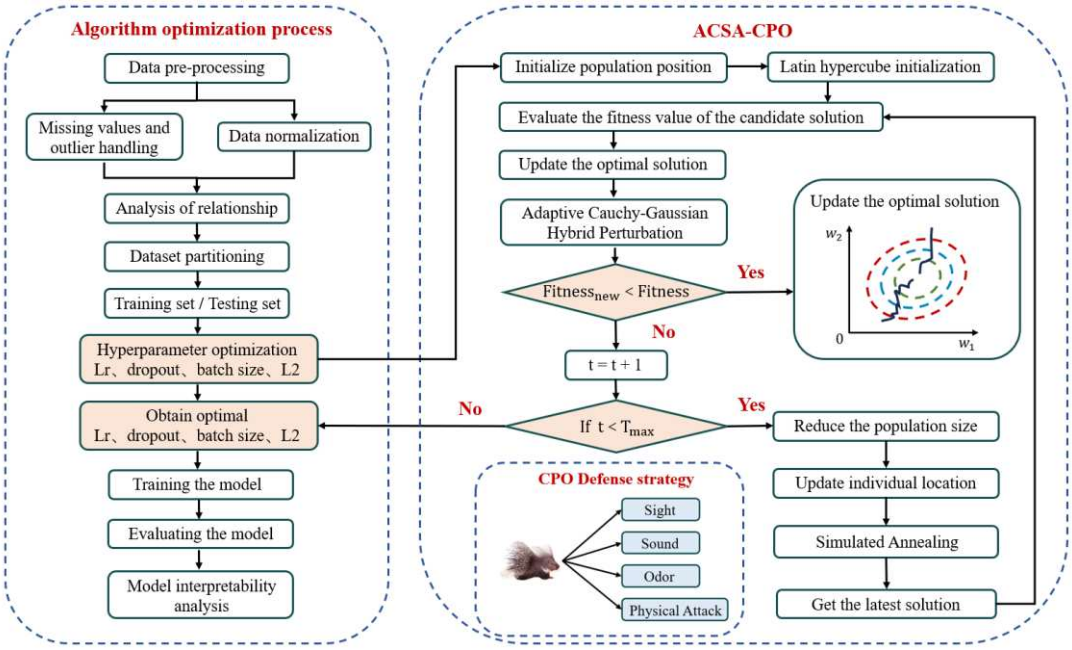


Figure 2.5 Overall Flowchart of Hyperparameter Optimization

2.7 Evaluation Metrics

To better evaluate and verify the accuracy of the ACSA-CPO-CNN-LSTM model in estimating reference evapotranspiration, this paper introduces Mean Absolute Error (MAE), Root Mean Square Error (RMSE), coefficient of determination (R^2), Mean Absolute Percentage Error (MAPE) and Nash-Sutcliffe Efficiency (NSE) according to the evaluation metrics commonly used in such models [29]. The specific calculation formulas are expressed as Formulas (27)-(31). Among the evaluation metrics, MAE directly reflects the absolute average level of prediction error; RMSE emphasizes the penalty for large errors and is sensitive to extreme errors; (R^2) is used to measure the proportion of the model explaining the variability of the target variable; MAPE provides percentage error for cross-scale comparison; NSE evaluates the fitting degree of the dynamic trend between predicted values and observed values, and is commonly used in hydrological model performance evaluation [30].

$$MAE = \frac{1}{n}\sum_{i=1}^{n}|y_i - \hat{y}_i| \tag{27}$$

$$RMSE = \sqrt{\frac{1}{n}\sum_{i=1}^{n}(y_i - \hat{y}_i)^2} \tag{28}$$

$$R^2 = \frac{[\sum_{i=1}^{n}(y_i - \bar{y}_i)(y_i - \hat{y}_i)]^2}{\sum_{i=1}^{n}(y_i - \bar{y}_i)^2 \sum_{i=1}^{n}(y_i - \hat{y}_i)^2} \tag{29}$$

$$MAPE = \frac{1}{n}\sum_{i=1}^{n}\left|\frac{(y_i - \hat{y}_i)}{y_i}\right| \times 100\% \tag{30}$$

$$NSE = 1 - \frac{\sum_{i=1}^{n}(y_i - \hat{y}_i)^2}{\sum_{i=1}^{n}(y_i - \bar{y}_i)^2} \tag{31}$$

Where y represents actual observation data, $\hat{y}$ represents prediction data, n represents the total number of samples, and $\bar{y}$ represents the average value of input samples.

2.8 Interpretability: SHAP

Shapley Additive Explanations (SHAP) is a model interpretation method based on Shapley values, used to evaluate the contribution of each feature to the model output, thereby explaining the "black-box model" from the global and local levels [31]. The calculation method of Shapley value is as follows:

$$\phi_i(f) = \sum_{S \subseteq N \setminus \{i\}} \frac{|S|!\,(|N| - |S| - 1)!}{|N|!}[f(S \cup \{i\}) - f(S)] \tag{32}$$

Where $\phi_i(f)$ is the Shapley value of feature i, S is a subset of the feature set, N is the complete set of all features, and $f(S)$ is the estimated output value of the model trained on feature set S

SHAP provides a unified method to explain the estimation results of any type of machine learning model [32]. In practical applications, since calculating Shapley values for all possible feature combinations becomes very complex and costly when the number of features is large, Monte Carlo simulation is usually used to approximate Shapley values. The calculation formula is as follows:

$$\hat{\phi}_{\{i\}}(f) = \frac{1}{M}\sum_{k=1}^{M}\phi_{k,x_i} \tag{33}$$

Where $\hat{\phi}_{\{i\}}(f)$ is the Monte Carlo simulation estimate of the Shapley value of feature x_i, M is the number of feature permutations used in Monte Carlo simulation, and ϕ_{k,x_i} is the Shapley value of feature x_i under the k-th permutation.

3. Experimental Research

3.1 Study Area and Data Sources

The study area is located in Changchun City, Jilin Province, Northeast China (125° 25'E, 43°

45'N), as shown in Figure 3.1. It belongs to a temperate continental monsoon climate zone, with an annual average temperature of 5.4° C and an annual average precipitation of about 600 mm. Rainfall is mainly concentrated in July to August, and precipitation shows a decreasing trend from east to west [33].

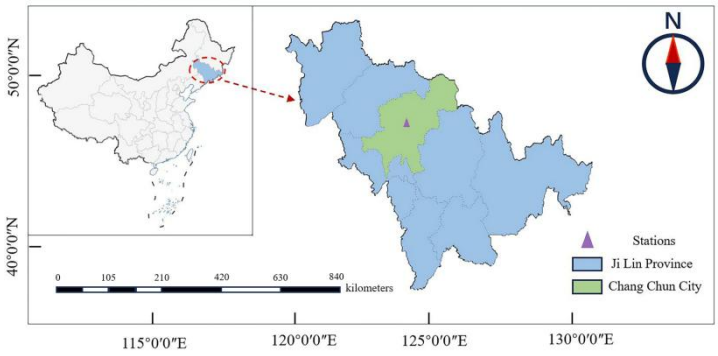


Figure 3.1 Geographic Location

Table 3.1 lists the input and output variables used in this study. All meteorological variables are derived from the ERA5 reanalysis dataset, and their main driving factors are selected as model inputs based on the physical mechanism of the Penman–Monteith (PM) equation, including a total of 9 variables such as air temperature, relative humidity, wind speed, solar radiation and precipitation. Among them, precipitation (P) is introduced as an auxiliary input variable to characterize the indirect regulatory effect of regional water conditions on reference evapotranspiration, thereby enhancing the model's adaptability to actual environmental changes. It should be pointed out that this paper does not simply take the PM formula as the fitting object, but takes its physical driving factors as prior constraints to construct a data-driven model for approximate estimation of reference evapotranspiration. Therefore, the selection of input variables not only reflects the physical basis of the PM equation, but also provides data support for the subsequent model to learn the complex nonlinear mapping relationship between meteorological elements and ET_o.

Table 3.1 Input and output variables

Feature	Full name	Unit
T_{max}	Maximum air temperature	℃
T_{avg}	Average air temperature	℃

Feature	Full name	Unit
T_{min}	Minimum air temperature	℃
RSG	Solar radiation	KJ/m²/day
RH_{max}	Maximum Relative humidity	%
RH_{avg}	Average Relative humidity	%
RH_{min}	Minimum Relative humidity	%
WS	Mean wind speed	m/s
P	Precipitation	mm/day
ET_o	Reference evapotranspiration	mm/day

The Pearson correlation analysis results between variables are shown in Figure 3.2. Overall, there are varying degrees of correlation between each meteorological variable and ET_0, providing a statistical basis for the rationality of model input variables. Among them, solar radiation and air temperature are significantly positively correlated with ET_0, while relative humidity is negatively correlated, which is consistent with the evapotranspiration physical mechanism described by the PM equation, indicating that the data distribution has good physical consistency. In addition, some variables (such as wind speed) have relatively weak linear correlation with ET_0, but this does not mean that their impact can be ignored, but indicates that their effect on the evapotranspiration process may have significant nonlinear and temporal coupling characteristics. Traditional empirical formula-based methods are difficult to effectively characterize such complex relationships, while the CNN-LSTM model constructed in this paper can adaptively extract local dynamic features and long-term dependency information from multivariate time series, thereby achieving efficient estimation of ET_0. This further reflects the effective supplementary role of data-driven methods to physical models under complex meteorological conditions.

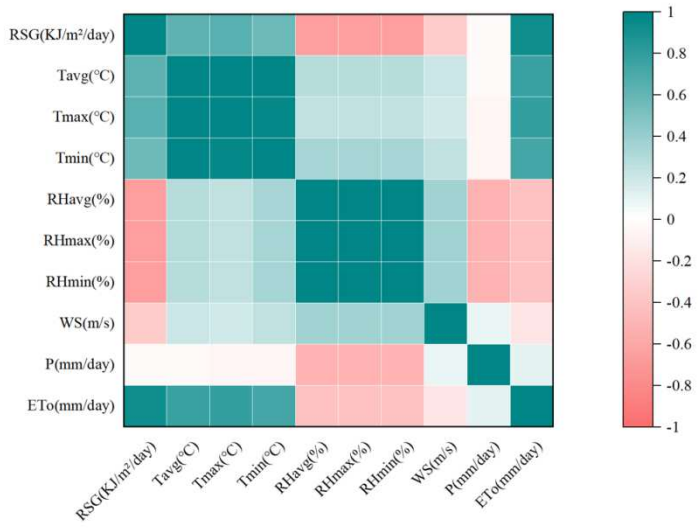


Figure 3.2 Heatmap of Pearson Correlation Coefficients between Variables

3.2 Data Preprocessing

3.2.1 Dataset Partitioning

To avoid potential information leakage in the time series modeling process and ensure the objectivity and reliability of model evaluation results, this paper adopts a time-order-based data partitioning method instead of random sampling. The research data covers daily meteorological data of Changchun, Jilin Province from 2020 to 2025. According to chronological order, the first 70% of the data is used as the training set for model training, and the last 30% is used as the test set for model performance evaluation, as shown in Figure 3.3.

It should be emphasized that although this paper uses the ET_0 calculated by the PM formula as the reference baseline value, the model training process strictly follows the causal structure of time series, ensuring that only historical meteorological information is used to estimate future ET_0, thus avoiding the information leakage problem of "directly fitting the target value based on variables at the same time". This partitioning method can more realistically simulate the scenario of rapid ET_0 estimation based on historical observation data in practical applications, improving the model's generalization ability and application value in real environments.

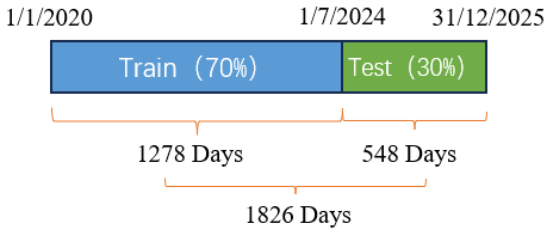


Figure 3.3 Dataset Division

3.2.2 Missing Value and Outlier Handling

To ensure data quality and improve the stability of model training, this paper conducts systematic missing value and outlier analysis on each meteorological variable (such as temperature, relative humidity, solar radiation, etc.). Statistical results show that there are only a small number of missing values in the data (accounting for less than 5%), so the linear interpolation method is used for filling to maintain the continuous characteristics of time series. For outlier handling, screening is carried out according to the physically reasonable range of meteorological variables. For abnormal data beyond the reasonable range, the boundary truncation method is used for correction to avoid interference of extreme outliers on the model training process.

The above processing not only improves data quality, but also ensures that input data conform to meteorological physical laws, so that the model focuses more on the real response relationship between meteorological elements and ET_0 during the learning process, rather than overfitting to abnormal noise. This is of great significance for constructing a data-driven estimation model with physical consistency.

3.2.3 Data Standardization

To eliminate the influence of dimensional differences between different meteorological variables on the model training process and improve model convergence speed and numerical stability, this paper adopts the Min-Max standardization method for input variables, scaling each variable to the [0,1] interval. The calculation formula is as follows:

$$X_{norm} = \frac{X - X_{min}}{X_{max} - X_{min}} \tag{34}$$

Where X_{norm} is the normalized value, X is the original value, and X_{max} and X_{min} represent the maximum and minimum values of the feature respectively. It should be pointed out that data standardization only acts on input meteorological variables, while the target variable ET_0

retains its physical dimension (mm/day) to ensure that the model output has clear physical significance. This processing method enables the model to not only improve numerical calculation efficiency during the learning process, but also maintain the interpretability of output results, thus better meeting the actual needs of reference evapotranspiration estimation tasks.

4. Experimental Results and Discussion

To comprehensively evaluate the performance of the ACSA-CPO-CNN-LSTM model in the ET_0 estimation task, this paper introduces multiple evaluation metrics to quantitatively analyze the model's estimation accuracy and generalization ability based on the PM formula calculation results as the reference baseline value, thereby verifying the effectiveness and stability of the proposed method in the data-driven approximate estimation task.

4.1 Experimental Results

Figure 4.1 shows the model training process. Taking MAE as the loss function, the model decreases rapidly in the first 50 epochs and tends to stabilize after about 120 epochs, indicating that the model has completed effective learning of the mapping relationship between meteorological variables and ET_0 and reached a convergence state.

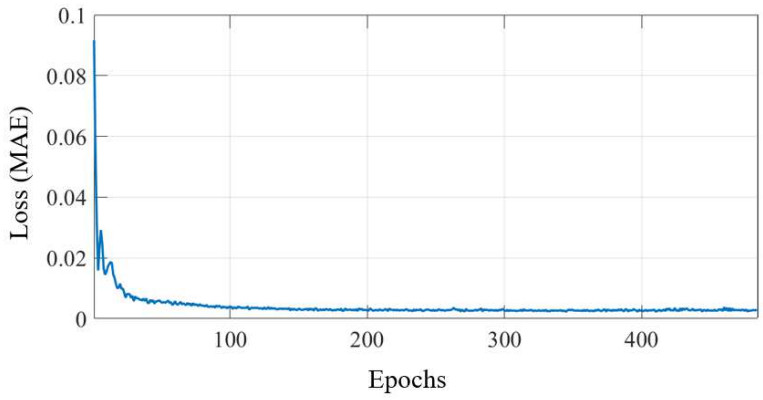


Figure 4.1 Iteration Loss Curve

Figure 4.2 shows the scatter distribution between the model estimated values and the reference values (ET_0 calculated by PM). The results show that most sample points are distributed near $y = x$ without obvious systematic deviation, indicating that the constructed model can conduct high-precision approximate estimation of ET_0 under the constraints of the PM physical benchmark. The coefficient of determination R^2 of the model reaches 0.8713, indicating that it can effectively characterize the main trend of evapotranspiration changes, and realize the approximate

reconstruction of ET_0 by learning the nonlinear coupling relationship between meteorological driving factors. This method not only maintains physical consistency, but also has stronger computational efficiency and adaptability to incomplete data.

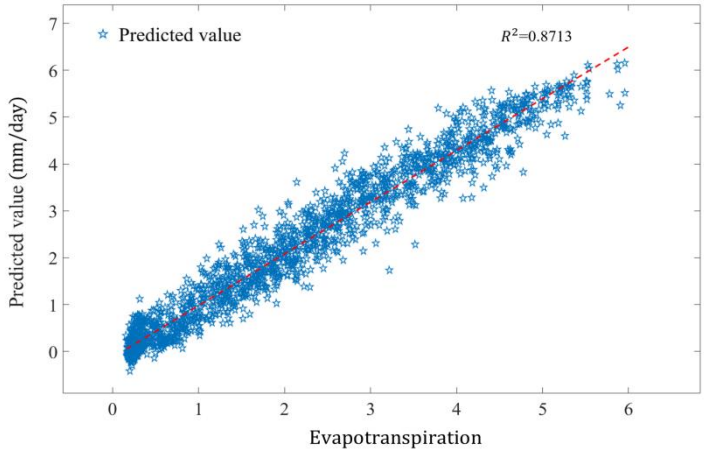


Figure 4.2 Prediction Performance Plot of Reference Evapotranspiration (ET_0)

Figure 4.3 shows the comparison of estimation results on the training set and test set. The model shows high consistency on both types of data without obvious overfitting. The residual distribution shown in Figure 4.4 is symmetric as a whole and concentrated near the zero value (about [-2, 2] interval), indicating that the model error mainly comes from random fluctuations rather than systematic deviation, further verifying the stability and generalization ability of the model.

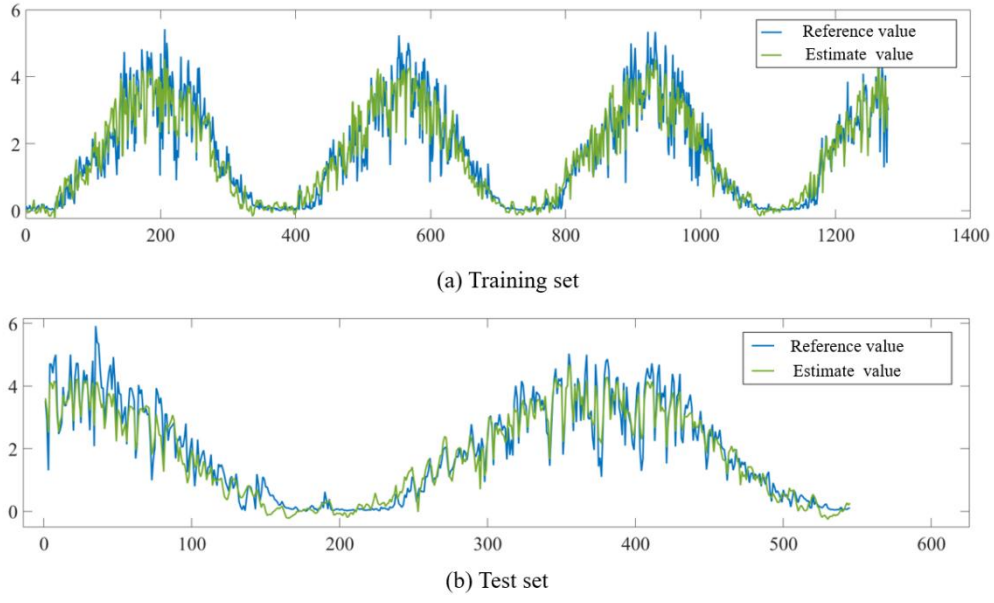


Figure 4.3 Comparison of Prediction Results in the Training Set and Test Set

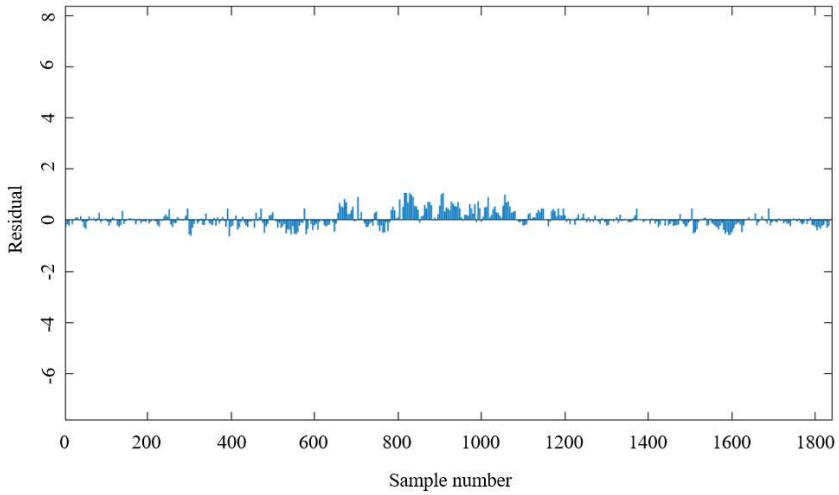


Figure 4.4 Residual Distribution Plot

Table 4.1 and Figure 4.5 further compare the performance of different models. The results show that the ACSA-CPO-CNN-LSTM model achieves the lowest values in error metrics such as MAE, RMSE and MAPE, and shows superior performance in R^2 and NSE metrics. Among them, MAE is 1.753 mm/day, which is about 11.2% lower than that of the CPO-CNN-LSTM model and more than 30% lower than that of the CNN model. The above results indicate that optimizing the hyperparameters of the CNN-LSTM model through a multi-strategy optimization algorithm can significantly improve the model's ability to model complex meteorological nonlinear relationships, thereby improving ET_0 estimation accuracy, rather than relying solely on the model structure itself.

Table 4.1 Evaluation metric results

Model	MAE (mm/day)	RMSE (mm/day)	MAPE (%)	R^2	NSE
CNN	2.547	3.247	40.3	0.7153	0.708
LSTM	3.875	4.962	56.7	0.4435	0.437
CNN-LSTM	2.132	2.896	25.6	0.8024	0.795
CPO-CNN-LSTM	1.975	2.439	24.1	0.8272	0.813
ACSA-CPO-CNN-LSTM	1.753	2.174	18.3	0.8713	0.859

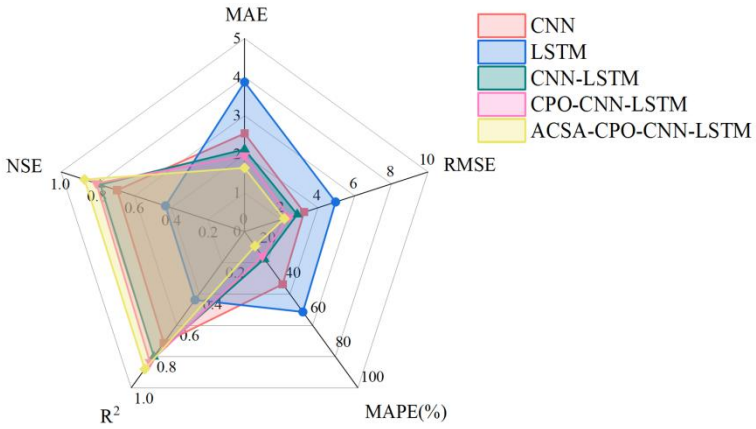


Figure 4.5 Comparison of Evaluation Indicators

4.2 Ablation Experiment

To evaluate the contribution of each component strategy of ACSA-CPO to model performance, this paper designs ablation experiments by removing the Latin Hypercube Sampling (LHS), Adaptive Cauchy-Gaussian Hybrid Perturbation (ACGH) and Simulated Annealing (SA) modules respectively, and compares them with the traditional Adam optimization method.

As shown in Table 4.2 and Figure 4.6, the complete model (LHS+ACGH+SA) achieves the optimal results in all metrics. After removing the ACGH module, the model performance decreases most significantly, with MAE rising from 1.753 to 2.128 mm/day, indicating that this strategy plays a key role in enhancing global search capability and avoiding falling into local optima.

In addition, the complete model still has an improvement in R^2 compared with the optimal sub-combination (ACGH+SA), indicating that LHS initialization and SA acceptance criterion have a synergistic effect in improving search stability and population diversity. Compared with the Adam optimizer, the CPO-based multi-strategy optimization method shows better performance in all evaluation metrics, indicating that it can more effectively improve the model's parameter search ability in high-dimensional nonlinear problems. Mechanistically, ACSA-CPO establishes a dynamic balance between "global exploration - local development", enabling the model to more fully learn the complex mapping relationship between meteorological variables and ET_0, thereby improving estimation accuracy and robustness.

Table 4.2 Ablation experiment evaluation metric results

Model	MAE (mm/day)	RMSE (mm/day)	MAPE (%)	R^2	NSE

LHS+ACGH+SA	1.753	2.174	18.3	0.8713	0.859
LHS+ACGH	1.942	2.441	21.5	0.8147	0.813
LHS+SA	2.128	2.897	25.7	0.7897	0.741
ACGH+SA	1.867	2.315	19.8	0.8352	0.827
Adam	2.132	2.896	25.6	0.7661	0.742

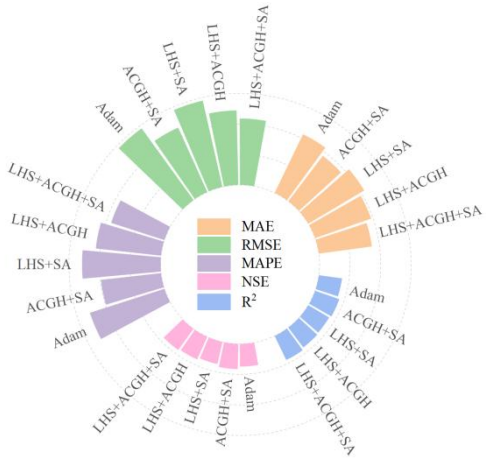


Figure 4.6 Comparison of Ablation Experiment Results

4.3 Horizontal Comparative Experiment

To further verify the effectiveness of the proposed method, this paper compares ACSA-CPO with typical optimization algorithms such as PSO, SSA and GWO. The results are shown in Table 4.3 and Figure 4.7. ACSA-CPO performs best in all evaluation metrics, among which MAE and RMSE are significantly lower than other methods, and R^2 and NSE also achieve the highest values. The results indicate that compared with traditional intelligent optimization algorithms, ACSA-CPO can more effectively balance global search and local convergence in the hyperparameter optimization process through a multi-strategy collaboration mechanism, thereby improving the overall model performance.

Furthermore, the performance differences of different optimization algorithms essentially reflect the differences in the model's ability to learn the nonlinear relationship of meteorological variables. The model optimized by ACSA-CPO can more accurately approximate the evapotranspiration process described by the PM physical model, and has stronger generalization ability and computational efficiency, verifying the advantages of the proposed method in the rapid reference evapotranspiration estimation task.

Table 4.3 Horizontal comparative experiment evaluation metric results

Model	MAE (mm/day)	RMSE (mm/day)	MAPE (%)	R^2	NSE

ACSA-CPO	1.753	2.174	18.3	0.8713	0.859
PSO	2.235	2.765	24.5	0.7837	0.772
SSA	1.983	2.596	20.8	0.8239	0.811
GWO	2.194	2.713	22.1	0.7949	0.785

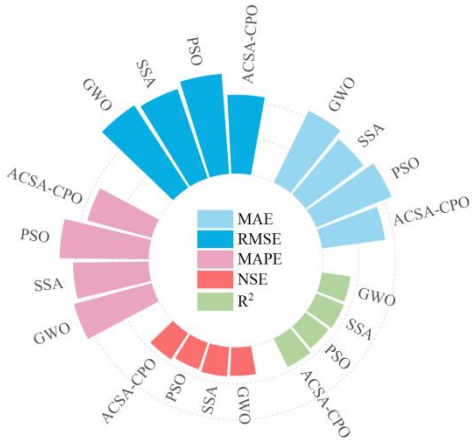


Figure 4.7 Comparison of Horizontal Comparison Experiment Results

4.4 SHAP-Based Interpretability Analysis

To further reveal the internal decision-making mechanism of the model and verify whether its estimation process conforms to the physical law of evapotranspiration, this paper introduces the SHAP (Shapley Additive Explanations) method to conduct interpretability analysis on the ACSA-CPO-CNN-LSTM model. Compared with traditional correlation analysis methods, SHAP can quantitatively decompose the marginal contribution of each input variable at the model level and characterize its nonlinear influence characteristics in different value ranges, thus providing a physical interpretation basis for the data-driven model.

As shown in Figure 4.8 and Figure 4.9, the impacts of different meteorological variables on ET_0 present significant nonlinear relationships. Taking air temperature as an example, its contribution is relatively limited in the low value range, while the SHAP value gradually increases with the rise of temperature, indicating that the evapotranspiration process is significantly enhanced under high temperature conditions. This change trend is highly consistent with the physical mechanism of evapotranspiration driven by energy. Relative humidity shows an overall negative contribution, and its SHAP value gradually decreases with the increase of humidity, but the change tends to be gentle in the high humidity interval, indicating that the inhibitory effect of humidity on evapotranspiration has a marginal weakening phenomenon within a certain range.

Solar radiation and wind speed show an overall positive contribution, and their impacts fluctuate with the change of values, reflecting the complex regulatory effect of meteorological variables on the evapotranspiration process under different environmental conditions. It should be emphasized that the SHAP analysis results not only reveal the nonlinear response characteristics of the model, but more importantly, the variable contribution trend is highly consistent with the physical mechanism described by the Penman–Monteith equation. This indicates that the constructed model does not simply perform numerical fitting on the PM formula, but reconstructs the physical response law of the evapotranspiration process under the data-driven framework by learning the internal coupling relationship between meteorological driving factors.

Figure 4.8 shows the feature importance ranking based on SHAP values. The results indicate that variables such as solar radiation, air temperature and wind speed play a leading role in ET_0 estimation, which is consistent with the contribution structure of energy term and aerodynamic term in the PM equation. The SHAP global influence diagram shown in Figure 4.9 further depicts the contribution changes of each variable in different value intervals, reflecting the model's adaptive response ability under different meteorological conditions.

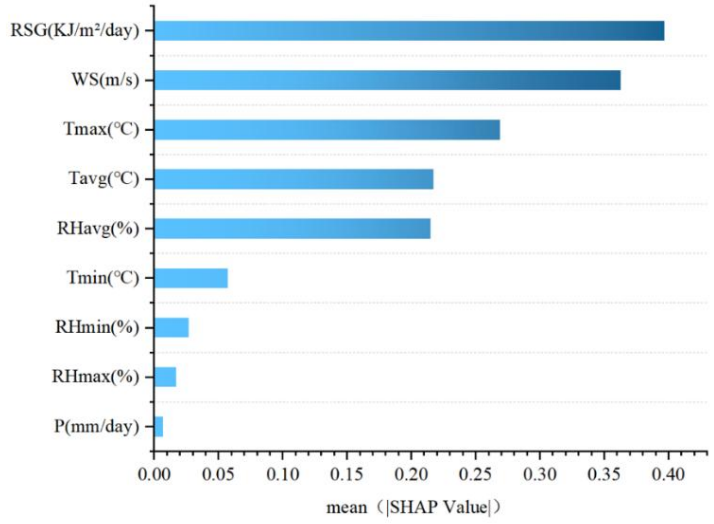


Figure 4.8 Feature Importance Ranking Based on SHAP Values

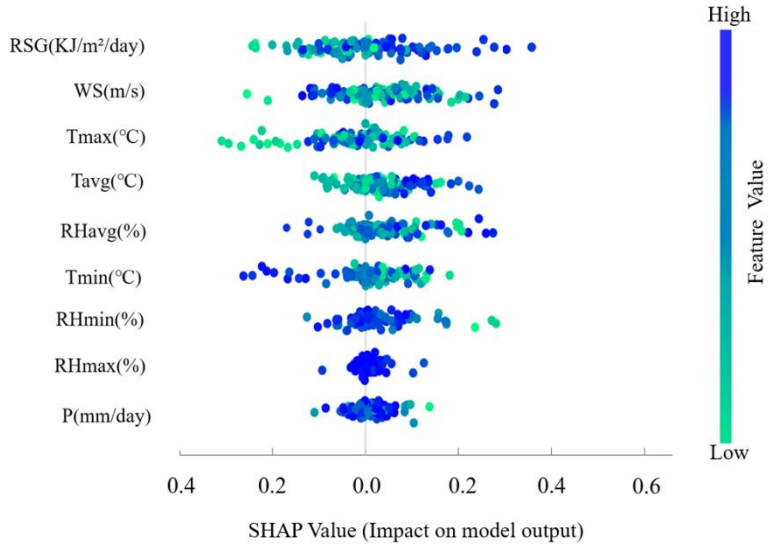


Figure 4.9 SHAP Global Feature Impact Plot

Overall, SHAP analysis not only provides an important basis for understanding the estimation behavior of the deep learning model, but also verifies the physical rationality of the model output results from the perspective of interpretability. The results indicate that the ACSA-CPO-CNN-LSTM model proposed in this paper not only maintains high-precision estimation ability, but also can balance physical consistency and interpretability, providing strong support for reliable estimation of reference evapotranspiration.

5. Conclusions

This paper proposes an ET_0 estimation model integrating ACSA-CPO and CNN-LSTM. Taking the PM formula calculation results as the reference baseline, the performance and mechanism of the proposed method are systematically verified through model construction, comparative experiments and interpretability analysis. The main conclusions are as follows:

(1) By introducing Latin Hypercube Sampling (LHS), Adaptive Cauchy-Gaussian Hybrid Perturbation (ACGH) and Simulated Annealing (SA) mechanism, the constructed ACSA-CPO algorithm achieves a dynamic balance between global exploration and local development. Experimental results show that compared with traditional CPO and Adam optimization methods, ACSA-CPO has stronger ability to jump out of local optima and convergence stability in high-dimensional complex search spaces, thus providing a better parameter configuration for the deep learning model.

(2) The CNN-LSTM model optimized based on ACSA-CPO is superior to the comparison

models in multiple evaluation metrics, among which MAE is 1.753 mm/day, about 11.2% lower than the unoptimized model and more than 30% lower than the single CNN model; meanwhile, R^2 reaches 0.8713 and NSE is 0.859, indicating that the model can effectively characterize the ET_0 change trend. The results show that the model can learn complex nonlinear relationships under multivariate meteorological conditions and achieve high-precision estimation of reference evapotranspiration.

(3) The analysis results based on the SHAP method show that solar radiation, air temperature and wind speed have significant positive contributions to ET_0, while relative humidity plays a negative regulatory role, and each variable shows obvious nonlinear influence characteristics in different value intervals. The above laws are consistent with the evapotranspiration physical mechanism described by the PM equation, indicating that the variable action relationship learned by the model under the data-driven framework has clear physical significance rather than simple numerical mapping.

(4) This paper takes key meteorological driving factors as physical prior constraints, and uses deep learning models to model the complex nonlinear relationship between meteorological variables and ET_0, so as to achieve efficient approximate estimation of the evapotranspiration process. Compared with traditional physical models, this method relies less on the integrity of input data while maintaining physical consistency, and has higher computational efficiency, suitable for scenarios with missing meteorological data or rapid calculation.

Overall, the ACSA-CPO-CNN-LSTM model proposed in this paper shows good performance in estimation accuracy, stability and interpretability, providing an effective method integrating optimization algorithm and deep learning for reference evapotranspiration modeling, and has certain application potential in agricultural water resource management and intelligent irrigation decision-making.

Despite achieving certain results, this paper still has some limitations. For example, the research data comes from a single region, and the spatial generalization ability of the model still needs to be further verified; in addition, the input variables are mainly meteorological elements, and key factors such as soil moisture and crop type have not been introduced. Future research can combine multi-regional and multi-source data to construct a spatiotemporal coupling model, and further integrate physical models and data-driven methods to improve the applicability and

robustness of the model.

Funding

No funding

References

[1] Lu, J., Geng, C., Cui, X., Li, M., Chen, S., Hu, T., 2021. Response of drip ferti gated wheat-maize rotation system on grain yield, water productivity and economi c benefits using different water and nitrogen amounts. Agric. Water Manag. 258, 107220.

[2] Ren, P., Huang, F., Li, B., 2022. Spatiotemporal patterns of water consumption an d irrigation requirements of wheat-maize in the Huang-Huai-Hai Plain, China and options of their reduction. Agric. Water Manag. 263, 107468.

[3] Wu, P., Wang, Y., Li, Y., Yu, H., Shao, J., Zhao, Z., Qiao, Y., Liu, C., Liu, S., Gao, C., Guan, X., Wen, P., Wang, T., 2023. Optimizing irrigation strategies for s ustainable crop productivity and reduced groundwater consumption in a winter wh eat-maize rotation system. J. Environ. Manag. 348, 119469.

[4] Guo, D., Olesen, J.E., Manevski, K., Ma, X., 2021. Optimizing irrigation schedule in a large agricultural region under different hydrologic scenarios. Agric. Water Manag.245, 106575.

[5] Ramos T B, Darouich H, Pereira L S. Mulching effects on soil evaporation, crop evapotranspiration and crop coefficients: A review aimed at improved irrigation management[J]. Irrigation Science, 2024, 42(3): 525-539.

[6] Gong Z, Gao F, Chang X, et al. A review of interactions between irrigation and evapotranspiration[J]. Ecological Indicators, 2024, 169: 112870.

[7] Dari J, Quintana-Seguí P, Morbidelli R, et al. Irrigation estimates from space: Im plementation of different approaches to model the evapotranspiration contribution within a soil-moisture-based inversion algorithm[J]. Agricultural Water Managemen t, 2022, 265: 107537.

[8] Pagano A, Amato F, Ippolito M, et al. Machine learning models to predict daily actual evapotranspiration of citrus orchards under regulated deficit irrigation[J]. Ec ological Informatics, 2023, 76: 102133.

[9] Zhang, Y.X., Zhao, Z.G., Zheng, J.H., 2020. Cat Boost: A new approach for esti mating daily reference crop evapotranspiration in arid and semi-arid regions of N orthern China. J. Hydrol. 588.

[10] Bakhshoodeh R, Ocampo C, Oldham C. Evapotranspiration rates and evapotranspir ative cooling of green façades under different irrigation scenarios[J]. Energy and Buildings, 2022, 270: 112223.

[11] Lankford B A. Resolving the paradoxes of irrigation efficiency: Irrigated systems accounting analyses depletion-based water conservation for reallocation[J]. Agricult ural Water Management, 2023, 287: 108437.

[12] Katimbo A, Rudnick D R, Zhang J, et al. Evaluation of artificial intelligence alg orithms with sensor data assimilation in estimating crop evapotranspiration and cr op water stress index for irrigation water management[J]. Smart Agricultural Tech nology, 2023, 4: 100176.

[13] Abeysiriwardana H D, Muttil N, Rathnayake U. A comparative study of potential evapotranspiration estimation by three methods with FAO Penman‐Monteith met hod across Sri Lanka[J]. Hydrology, 2022, 9(11): 206.

[14] Roy D K, Sarkar T K, Kamar S S A, et al. Daily prediction and multi-step forw ard forecasting of reference evapotranspiration using LSTM and Bi-LSTM models [J]. Agronomy, 2022, 12(3): 594.

[15] Li M, Zhou Q, Han X, et al. Prediction of reference crop evapotranspiration base d on improved convolutional neural network (CNN) and long short-term memory network (LSTM) models in Northeast China[J]. Journal of Hydrology, 2024, 645: 132223.

[16] Ali M, Nayahi J V, Abdi E, et al. Improving daily reference evapotranspiration f orecasts: Designing AI-enabled recurrent neural networks based long short-term m emory[J]. Ecological Informatics, 2025, 85: 102995.

[17] Chen J, Chen K, Zhu Y. Hybrid CNN-LSTM-Attention Model for Enhanced Refe rence Crop Evapotranspiration Estimation toward Optimized Irrigation Scheduling [J]. Journal of Agriculture and Food Research, 2025: 102545.

[18] Bamber S S, Katkuri A V R, Sharma S, et al. A hybrid CNN-LSTM approach f

or intelligent cyber intrusion detection system[J]. Computers & Security, 2025, 148: 104146.

[19] Zhao F, Li Z, Guo P, et al. Enhanced crested porcupine optimizer for numerical optimization and wireless sensor network deployment[J]. Scientific Reports, 2025, 15(1): 40141.

[20] Liu H, Zhou R, Zhong X, et al. Multi-strategy enhanced crested porcupine optimizer: CAPCPO[J]. Mathematics, 2024, 12(19): 3080.

[21] Han, X., Wei, Z., Zhang, B.Z., Li, Y.N., Du, T.S., Chen, H., 2021. Crop evapotranspiration prediction by considering dynamic change of crop coefficient and the precipitation effect in back-propagation neural network model. J. Hydrol. 596.

[22] Kaur G, Sinha R, Tiwari P K, et al. Face mask recognition system using CNN model[J]. Neuroscience Informatics, 2022, 2(3): 100035.

[23] Srinivasan S, Francis D, Mathivanan S K, et al. A hybrid deep CNN model for brain tumor image multi-classification[J]. BMC Medical Imaging, 2024, 24(1): 21.

[24] Luo J, Gong Y. Air pollutant prediction based on ARIMA-WOA-LSTM model[J]. Atmospheric Pollution Research, 2023, 14(6): 101761.

[25] Li Q, Guan X, Liu J. A CNN-LSTM framework for flight delay prediction[J]. Expert Systems with Applications, 2023, 227: 120287.

[26] Wen X, Li W. Time series prediction based on LSTM-attention-LSTM model[J]. IEEE access, 2023, 11: 48322-48331.

[27] Xu H, Wu L, Xiong S, et al. An improved CNN-LSTM model-based state-of-health estimation approach for lithium-ion batteries[J]. Energy, 2023, 276: 127585.

[28] Adalja D, Patel P, Mashru N, et al. A new multi objective crested porcupines optimization algorithm for solving optimization problems[J]. Scientific Reports, 2025, 15(1): 14380.

[29] Naidu G, Zuva T, Sibanda E M. A review of evaluation metrics in machine learning algorithms[C]//Computer science on-line conference. Cham: Springer International Publishing, 2023: 15-25.

[30] El-Kenawy E S M, Zerouali B, Bailek N, et al. Improved weighted ensemble learning for predicting the daily reference evapotranspiration under the semi-arid cli

mate conditions[J]. Environmental Science and Pollution Research, 2022, 29(54): 81279-81299.

[31] Song Z, Cao S, Yang H. An interpretable framework for modeling global solar radiation using tree-based ensemble machine learning and Shapley additive explanations methods[J]. Applied Energy, 2024, 364: 123238.

[32] Nohara Y, Matsumoto K, Soejima H, et al. Explanation of machine learning models using shapley additive explanation and application for real data in hospital[J]. Computer Methods and Programs in Biomedicine, 2022, 214: 106584.

[33] Du, C., Chen, J.S., Nie, T.Z., Dai, C.L., 2021. Spatial–temporal changes in meteorological and agricultural droughts in Northeast China: change patterns, response relationships and causes. Nat. Hazards 110(1), 155–173.